American Journal of Water Resources, 2023, Vol. 11, No. 2, 49-64
Available online at http://pubs.sciepub.com/ajwr/11/2/2
Published by Science and Education Publishing
DOI:10.12691/ajwr-11-2-2

Contribution of Remote Sensing and Geophysical Prospecting (1D) to the Knowledge of Groundwater Resources Burkina Faso

Faye Moussa Diagne*, Biaou Angelbert Chabi, Doulkom Palingba Aimé Marie, Koita Mahamadou, Yacouba Hamma

Laboratoire Eaux Hydro-Systèmes et Agriculture (LEHSA), Institut International d'Ingénierie de l'Eau et de l'Environnement (Institut 2iE), 1 Rue de la Science, 01 BP 594 Ouagadougou 01, Burkina Faso
*Corresponding author: moussadiagnefaye@gmail.com

Received May 02, 2023; Revised June 04, 2023; Accepted June 12, 2023

Abstract In Burkina Faso, the use of groundwater in a basement environment represents a major asset for rural populations, due to the questionable quality of surface water. It is exploited through boreholes installed with the help of 1D electrical geophysical investigations. Analysis of the database of 206 boreholes reveals that 30% are negative and 40% are unproductive or have a low flow rate of less than 2.5 m^3/h in the study area. This has an impact on the access rate, which was set at 80% in 2015, and which is 71.9% in 2015 and 76.4% in 2020. In view of this observation, in order to define the geometry of the aquifer and productivity, we propose to see whether the methodology (1D) presents certain limitations or difficulties in correlating the lineaments with the preferential water circulation corridors in this type of geological context. Does it also allow us to highlight the thickness and nature of the alteration? To achieve this, remote sensing is used followed by validation. Subsequently, possible correlations between the types of geophysical anomalies and the productivity of the boreholes were identified using a statistical analysis of the 206 boreholes. Geophysical prospecting was used to propose new drilling locations based on fracture directions.

Keywords: *hydrogeology, electrical profile, crystalline basement, remote sensing, water management*

Cite This Article: Faye Moussa Diagne, Biaou Angelbert Chabi, Doulkom Palingba Aimé Marie, Koita Mahamadou, and Yacouba Hamma, "Contribution of Remote Sensing and Geophysical Prospecting (1D) to the Knowledge of Groundwater Resources Burkina Faso." *American Journal of Water Resources*, vol. 11, no. 2 (2023): 49-64. doi: 10.12691/ajwr-11-2-2.

1. Introduction

Research and exploitation of groundwater in the middle of the bedrock has remained at the prospective stage compared to similar aquifers [1,2,3,4].

In this country, the average volume of water available is 850 m^3 per year per capita, slightly below the water scarcity threshold of 1000 m^3/year/hbt [5]. Groundwater in the basement environment represents a major asset in terms of drinking water for rural populations, as surface water is not perennial in addition to its often impure quality [6,7,8].

If the importance of fracturing is no longer to be demonstrated, the problem of fault location is not resolved, because it is strongly linked to geology and and climate change [9,10]. The Sissili sub-basin occupied by 12 municipalities and 3 provinces is one of these areas where groundwater is most often located in alterites and uses privileged corridors which are fractures. In the early 1970s, many works were aimed at studying tectonics. However, aerial photography was the most widely used and had certain limitations resulting from the difficulty of correlating lineaments to preferential water circulation corridors [11]. With the need to exploit groundwater felt by the growing population, a large number of boreholes are drilled every year to improve the water supply, but these remain costly and unsatisfactory, as 67 of the 206 boreholes surveyed are polluted, 30 have been abandoned by the population, 60 are negative and 83 with a productivity rate of less than 2.5 m^3/h [12]. Added to this, a climatic context where precipitation show high spatial variability with a downward trend [12,17].

The objective of this study is to help improve the mapping of hydraulically favorable fractures by remote sensing, which is essential, and geophysics, with the aim of improving the rate of positive drilling implantations without having too much impact on investment [17-21]. Through the profiles carried out, the geometry of the aquifer was defined. To do this, we will adopt linear mapping to define the rectilinear structures defining the groundwater corridor with statistical analysis. Then a validation will follow by geophysics (1D) with the

adaptation of the electrical resistivity method because the cuirass has a higher propagation speed than that of the underlying alterites. And finally a statistical analysis will be made to study the correlation which exists between the lineaments and the productivity of the works.

2. Materials and Methods

2.1. Study environment

The Sissili sub-watershed is located in southern Burkina Faso (Figure 1). It covers an area of 7559 km^2. It extends between longitudes 1° and 2° West and latitudes 11° and 12° North [12].

The relief is characterized in places by small rock masses. There are also small hills (elephant back), chaos of balls (granite) and barely marked hilltops. The average slope of the hydrological units is 2.03m/km, the overall slope index is 0.2m/km.

The catchment area Sissili includes 3 types of land use: agricultural areas, pastoral areas and wetlands. Agricultural areas include rainfed crops, crops under agroforestry parks or agroforestry territories, mosaics of fallow crops and large natural areas, and forest and irrigated plantations [22]. These are the most important from the point of view of spatial occupation. This tree cover is generally equal to or greater than 25% of the total area. Mosaic areas/natural spaces are vast expanses of natural formations (savannah or steppe) dotted with fields. These are pasture areas where small ruminants are mainly kept in the winter season. Its Sudanian-type climate (South Sudanese) located south of the 11°30'N parallel, covers the entire catchment area Sissili. It is characterized by an average annual rainfall greater than 900 mm; a rainy season that lasts more than 6 months of the year, fairly low annual thermal amplitudes Direction de la Météo, (2001).

Hydrographically, the study site is crossed by the Sissili River (tributary of the Nazinon) which gives its name to the province (area). It is 322km long with an average gradient of 1.48m/km over the first 42 km.

From a geological point of view, the formations encountered are varied and can be grouped into two major geological units of Proterozoic ages: the plutonic unit and the sedimentary volcano unit [19,23,24,25]. At the hydrogeological level, hydraulic productivity is defined by geological formation. Plutonic formations such as granodiorites, tonalites and quartz diorites have the highest hydraulic productivity with permanent flowsthat can exceed 20 m^3/h. Then follow formations such as orthogneiss, kyanite micaschists, garnet leptynites, garnet micaschists, sillimanites and staurolites which show an average productivity of around 20 m^3/h.

Low hydraulic productivities are generally encountered in sedimentary volcano formations. It can exceed 5 m^3/h but this can drop due to clogging. While the weakest are at the level of intrusive plutons and can hardly reach 2 m^3 /h [12].

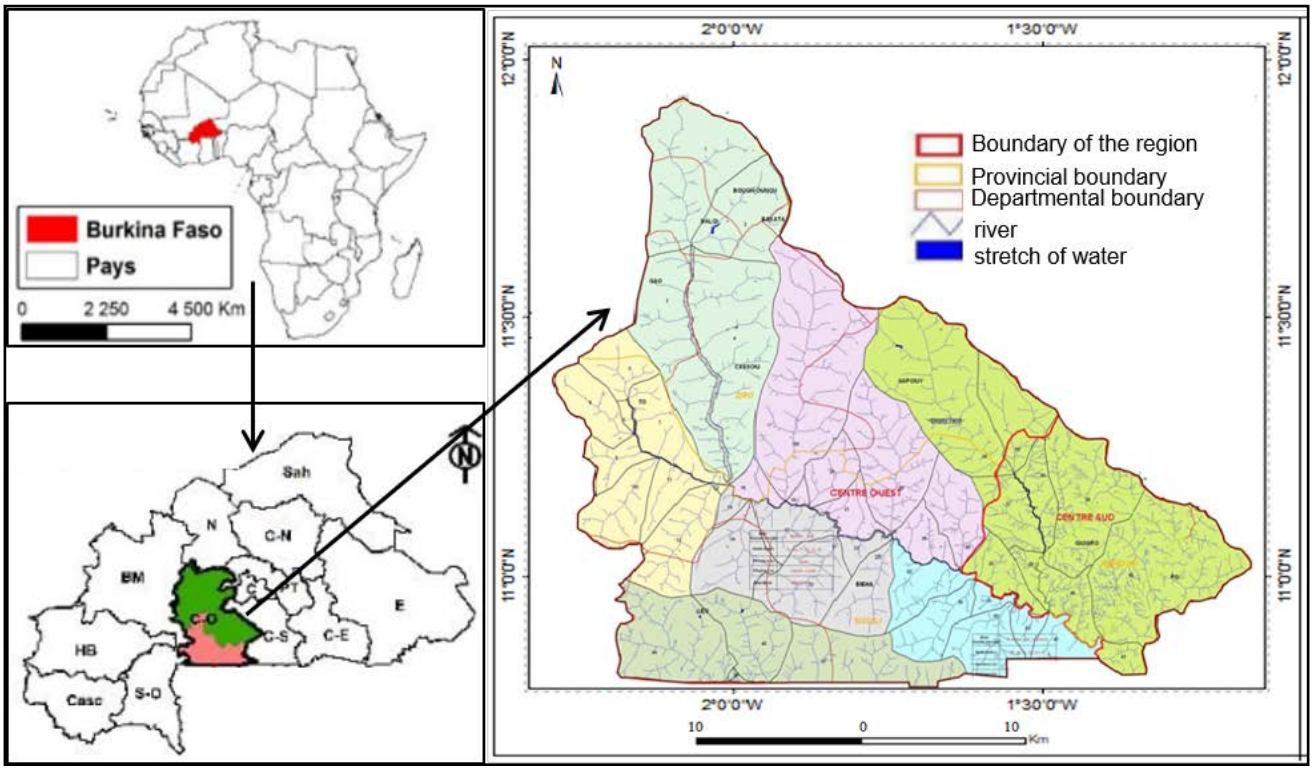

Figure 1. Localization of the study zone of study

2.2. Data Processing from Remote Sensing Method

In this work, it is through Landsat satellite imagery to map the distribution of lineaments in the basement zone in order to analyze the role of fracturing in the circulation of underground water. Authors like [26-30] recommend the use of satellite imagery, particularly Landsat 8 images, for a good study of water resources in the basement zone. These images of scenes 195 (052-053) composed of 11 bands and acquired in February 2014, generally appear clear because this period of the year corresponds to the dry period. Added to this is the combination of the geological and topographic map. To do this, the processing was done in two phases: the fusion of the images because the study area does not fit on a single image [31-35] and the application of the filters [26,36-40]. The structures identified were the subject of a frequency analysis and the directions compared with those of the recorded discontinuities. These pre-processed satellite images have undergone corrections and processing. Then they were grouped by class of 10° in 10° for their statistical processing, with the aim of obtaining classes of preferential directions which are reported on the rosette of directional distribution [27,30,41,42]. Thus with the Envi software, the ACP made it possible to merge the OLI bands (multi-spectrum and infrared) for the purpose of improving image quality, removing redundant information and compiling data. A second ACPS is then carried out with the infrared bands. The resampling of the pixels of the panchromatic bands was additionally necessary to bring the pixels from 60 m to 30 m side [43,44,45]. The application of Principal Component Analysis (PCA) on the Sobel filters allowed an enhancement lineaments associated with megastructures and large shear corridors. A visual analysis has eliminated all kinds of false presentations [46]. These different bands also allowed the application of the technique of fusion by RGB coding which makes it possible to compose the final image. It is for example necessary to attenuate the blue channel (OLI1), in the composition OLI 2 and 3, because its level is artificially increased by atmospheric Rayleigh scattering. The Sobel filters made it possible to identify a few lineaments. In practice, the 7×7 Sobel filters (assigned the weight 6) in the NS directions; EO, NE-SW and NW-SE were used in this study. The highlighting of the following Landsat 8 lineaments was possible thanks to the highlighting of the ratios (OLI5/OLI6; OLI5/OLI4; OLI7/OLI4; OLI6/OLI5). We also used the ARSIS method described by [47], to identify the normalised vegetation index.

2.3. Manual Extraction of Lineaments by Visual Analysis Method

It is advisable to apply it on the colored composition to see the variation of the gray tone. Then we proceed to manual surveys. This consists in symbolizing by a straight section the image discontinuities and the sudden changes in tonality observed on the processed images. [48] recommends a length of 280 m for surveys, whereas [49] takes 9 km as major lineaments and 480 m for small lineaments. This was possible thanks to the software Geomatica for the extraction of lineaments [42,50], Rockwork to calculate the extracted directions in number and length [51,52]. The lineaments identified from the Landsat images were the subject of a frequency analysis making it possible to highlight the main directions using the directional rosette [53]. The lineaments thus observed can be closed or open fractures; subvertical or reverse faults; veins generally associated with fractures; geological contacts; the foliation of metamorphic rocks especially as the fractures follow the foliation planes.

2.4. Validation of the Lineament Map Method

For validation, the literature has shown us several types. The first refers to superimposing the directional rosette map which has been the subject of a frequency analysis making it possible to highlight the main directions then compare them to those of previous work carried out in the Sissili sub-basin [19,54]. According [55], observation on different supports, at different scales and by different photo-interpreters, can lead to the consideration of lineaments as effective fractures in the field, [56] used this technique in his study area and thus had a correlation by comparison. Subsequently, it was a question of superimposing productive boreholes according to the CIEH classification and negative ones already drilled in the study area on the lineament map. This gave us an indication of the preferred directions. The methodology consisted of a comparative analysis of the electrical prospecting results with the drilling logs. This analysis was carried out by grouping the prospecting measurements into families of geological formations encountered in the study area. And finally the validation is completed by a geophysical survey (1D). The objective of the trail is to determine the variation in apparent resistivity for a given depth of investigation in order to understand the increase in the roof of the substratum. It is shown not to effectively establish the thickness of the weathered aquifer. Subsequently, in addition, soundings will be established, the purpose of which is to define the vertical classification of the apparent resistivities. As a result, through in-depth research, he agrees to travel through the different formations to determine the thicknesses of the terrain. In the case of the validation of lineaments for the implantation of HandPumps, a single profile is often sufficient, especially in the case of green rocks or migmatites. But in this study, we opted to make parallel profiles to see the direction of the fractures and then compare it with the position of the productive and negative boreholes. Sequences acquisition of data are programmed under the Prosys II software with a Schlumberger device as shown in Table 1. Then using the IP2WIN software, we interpreted the data in terms of resistivity and thickness in order to characterize and quantify the thicknesses of the underlying lands. In this study, a total of 12 drags (3 profiles per site) and 5 boreholes were carried out in order to improve the implantation of the boreholes as shown in Figure 2. The choice of measurement sites in the sub-basin was made taking into account the different geological formations present in the study area. This will allow us, after validation, to group the two categories of positive and negative drilling according to the type of formation.

Table 1. Characteristics of drag profiles

Site	Koukin	Kada	Sissili Mossi	Tiakane
Distance (m)	860	400	400	400
AB/2 (m)	200	200	200	200
NM (m)	10	10	10	10

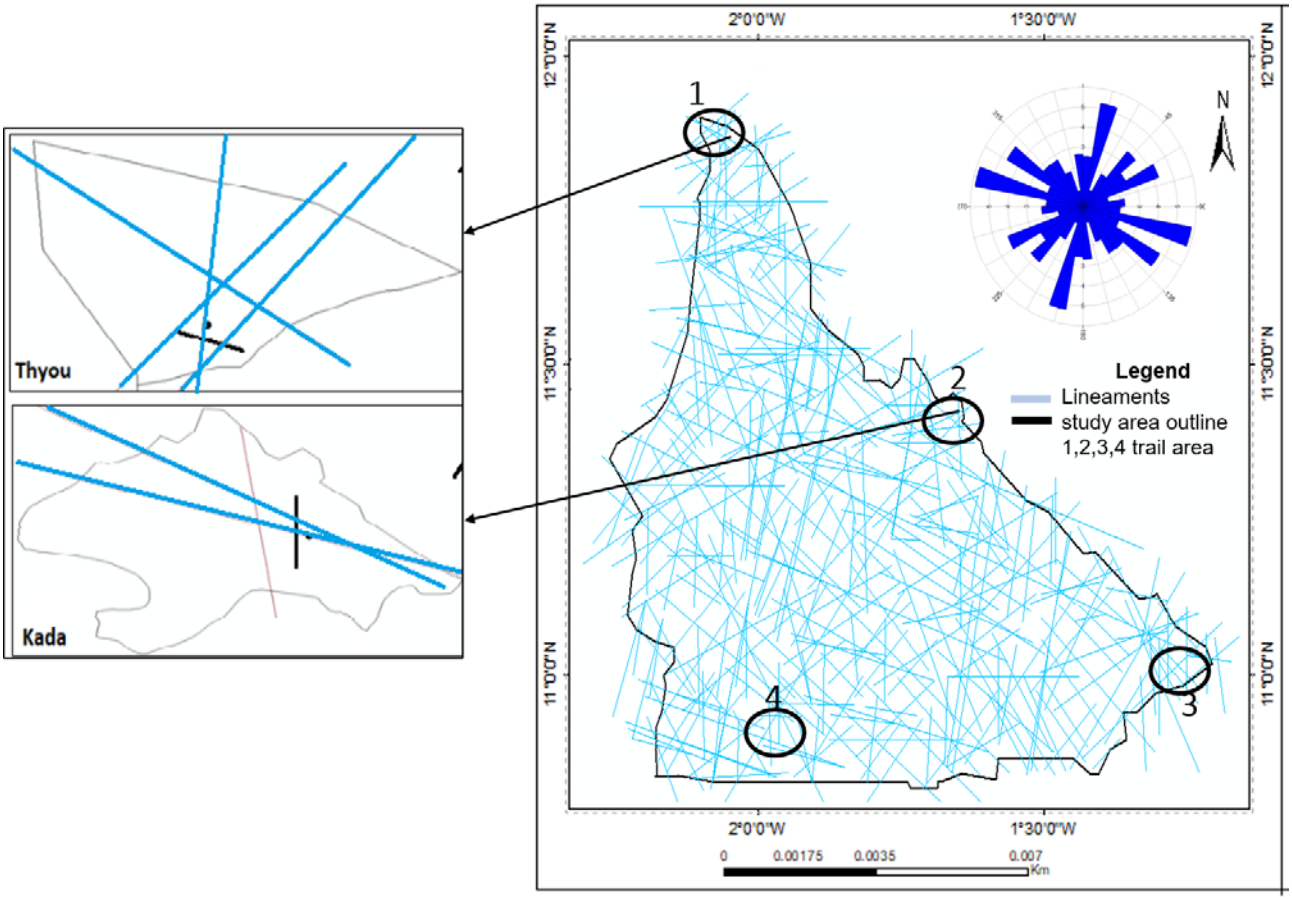

Figure 2. Presentation of electrical profile zones in the municipality of Kada and Sapouy

2.5. Data Processing from the Statistical Analysis Method

Based on the cross tables, the first step is to find the correlation between the qualitative parameters and the hydrogeological parameters; and thus to visualize the data in 2D then to link the elements of the same character according to their negative or positive state. Thus, we will determine the rate of success and failure according to the type of formation, the form of anomaly, and the direction of the fractures.

2.6. Estimation of the Distance of Boreholes Fractures and Flow Classes Method

The parameters related to hydrogeology were obtained from the technical sheets of 206 positive and negative boreholes. The proposed technique consists in estimating the distance between positive boreholes - lineaments, negative boreholes - lineaments and the flow classes - lineaments, while putting the relationships that remain between the major discontinuity and the flow rates (Q) of the boreholes. The flow classification adopted is that of the CIEH: [0−1 m^3/h] Very low, [1−2.5 m^3/h] Low, [2.5−5 m^3/h] Medium, [>5 m^3/h] High.

3. Results and Discussion

3.1. Image Processing

3.1.1. Data Processing from Remote Sensing

The identification of the main corridors was possible thanks to the analysis of certain processed images. These images also allow the vectorization of the hydrographic network and possibly the geological accidents attached to it [49]. The ACP (Figure 3), very clearly draws a domain in a fine gray tone in the southwestern part. And the lineaments of NE-SW and NS direction defined by the regional accident are clearly visible there. The Sobel filters on the raw image channels of Landsat 8 OLI3/OLI4 (Figure 4) make it possible to identify the means for recognizing hitherto poorly known lineaments and corresponding to lithological or structural discontinuities in the images by causing an effect shadow optics cast on the image [57]. The NS-trending Sobel filter maintains structural cracks and accurately EW, NO-SE (Liberian) and NE-SW (Eburnean) trending lineaments [58]. We also note that certain lineaments governing the direction of different water arms in the region correspond to parallel faults that

probably have the same geological history. This methodology resulted in the visualization of many discontinuities, sometimes kilometric and materialized by dark and gray areas of direction N°10-20. Many other additional regional accidents have been highlighted and identified from the analysis of certain colored compositions. Analysis of this detailed lineament map reveals that almost all of the hectometer-sized lineaments follow either the NW-SE direction or the NE-SO direction. These fractures are much sought after during hydrogeological prospecting for the search for underground water [27].

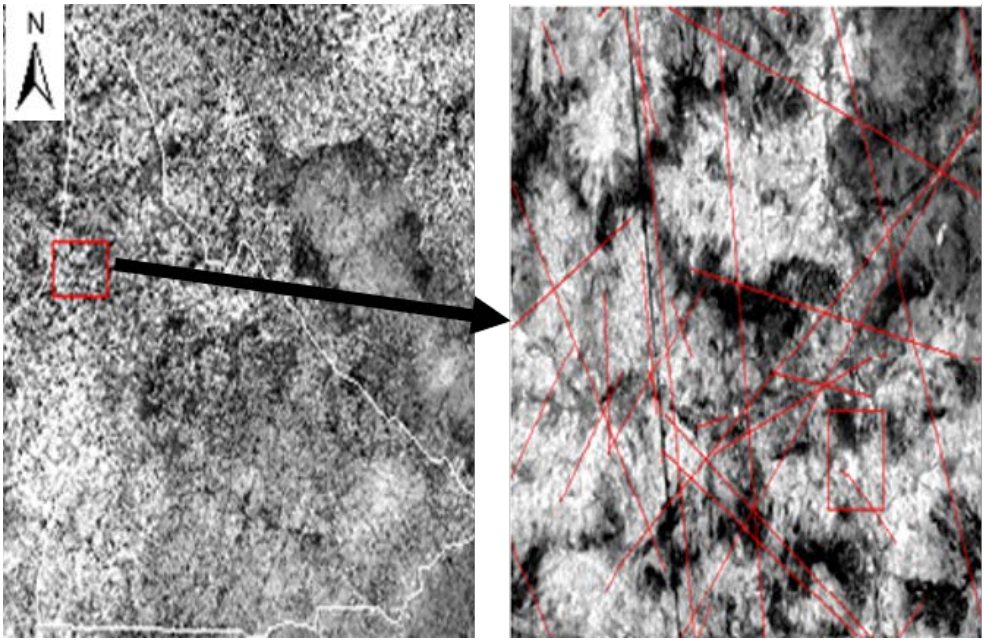

Figure 3. Highlighting ACP lineaments

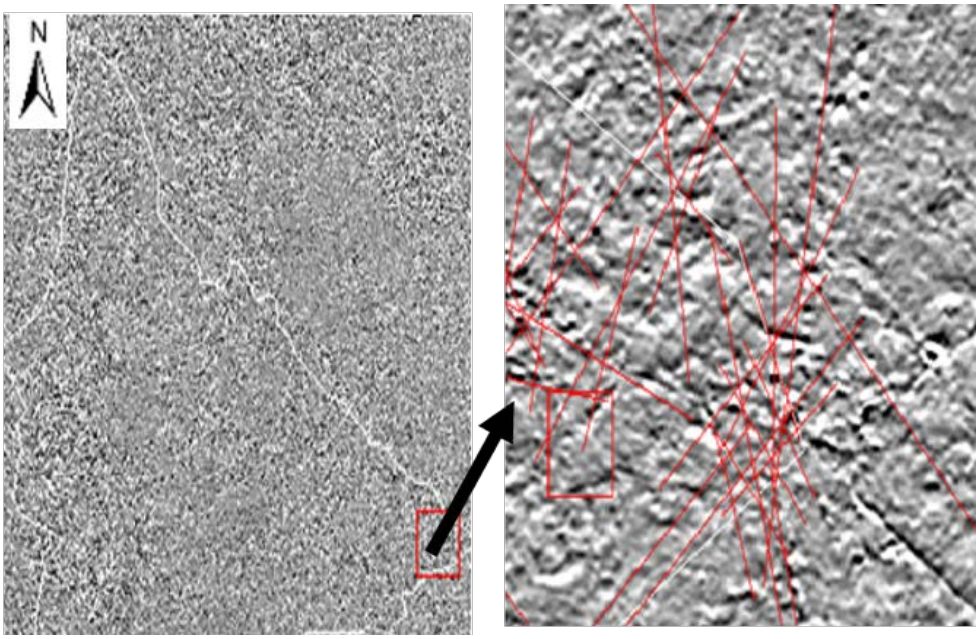

Figure 4. North South filter application

3.1.2. Manual Extraction of Lineaments by Visual Analysis

Lineaments were drawn by hand. Figure 5 represents the results obtained after extraction of the lineaments carried out on the Landsat images and its rosette to indicate the directions. Extraction of lineaments from satellite images reveals different sizes and directions. This confirms the tectonic studies carried out by [19] in Burkina who assert that the Sissili sub-basin would have been influenced by several tectonic phenomena which led to the pronounced fragmentation of the geological formations. There is a large representation of the major directions of the NO-SE and NE-SW family and a minority class of the NS and EO family. The directions given by the filters are superimposed on the geological map and show the Liberian (NS) and Eburnean (NE-SW) formations of the West African craton. This makes this map not complete, but very representative.

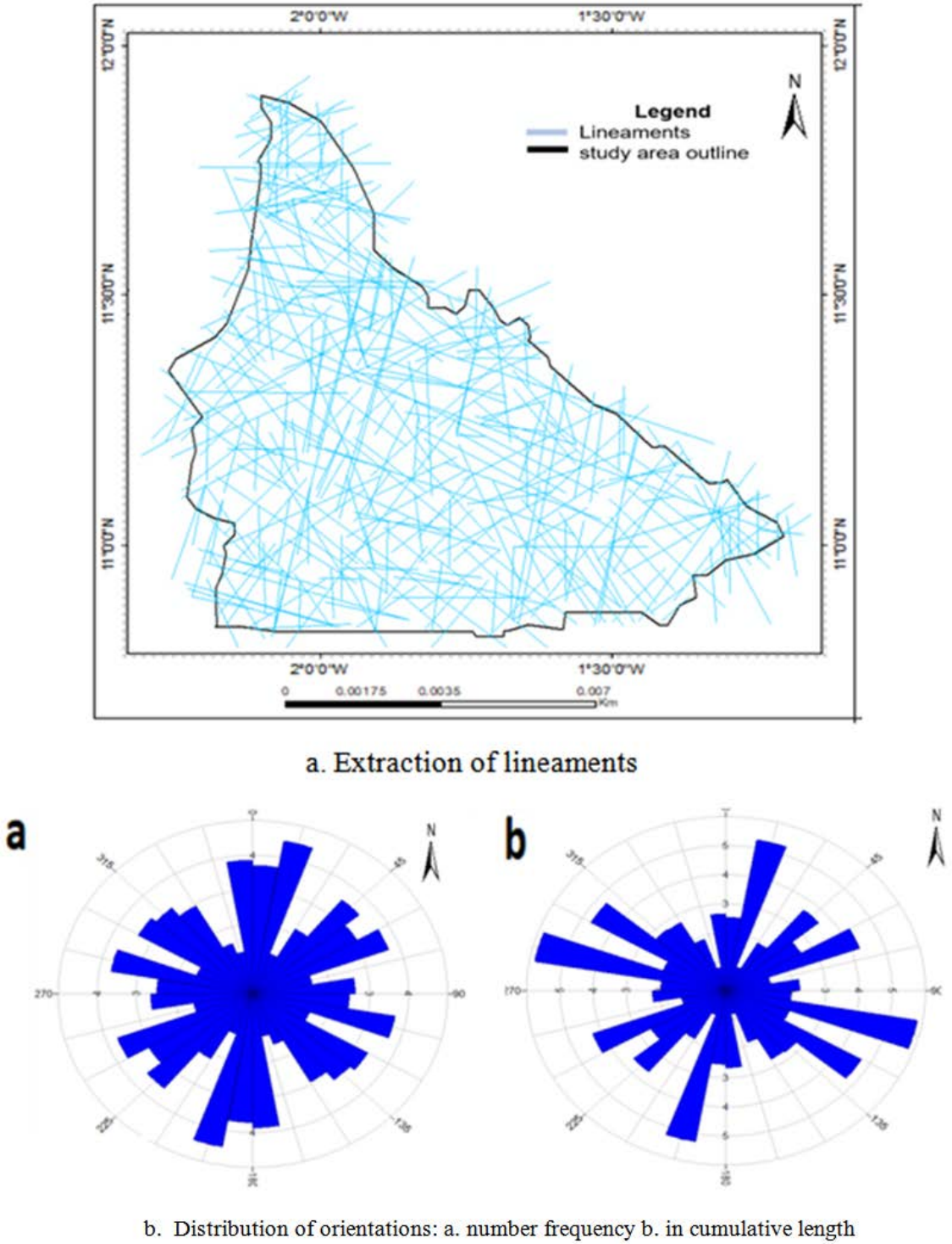

a. Extraction of lineaments

b. Distribution of orientations: a. number frequency b. in cumulative length

Figure 5. Map of lineaments from Landsat satellite images

3.2. Lineament Map Validations

3.2.1. Validation of the Lineament Map in Imaging: Overlay Directional Rosette Map

The directional rosettes from the Landsat images of this study and those from the aerial photography of [23] were analyzed by figure 6. It appears that the two rosettes have a fairly good correlation with directions N60°-70°, N140°-150° with frequency peaks. On the aerial photography, we find peaks in the vicinity of N10°, N20°, N40°, while at the level of our directional rosette of the Landsat images, it emerges from the preferential directions N10°-15°, N30°-35°, N185°-90°. The directions can be associated in pairs of directions N°10-20°, N°60-70°, N100°-110°. There are also non-existent directions on the N30°-N35°, N165°-N175° images, and in the aerial photography it is rather the N80° and N110° directions. This absence of direction can be explained by the fact that the satellite scans the East-West direction, which is visible on the aerial photography as well. The two maps present frequency peaks N40°-50°, N60°-70°, N120°-140° and directions which form perpendiculars (right angles) are visible there: N15°-105°,

N45°-135°, N60°-150. We can add to this that the hydraulic role of the different fractures makes it possible to distinguish between open and closed joints. By superimposing the boreholes on the lineaments, we notice several directions including N0°-N20°, N60°-N70° which represent the negative boreholes and therefore closed joints. Indeed, open joints at the surface can end up closed at depth causing a reduction in permeability and causing the disappearance of satellite lineaments at the same time as the reduction of voids. Others, on the other hand, in directions N90°-N100°, N120°-N130° and N160° represent positive boreholes and therefore open joints. It was retained that the open directions are the most capable of playing a drainage role with respect to the surrounding alterites. The difference in fracturing density recorded at the level of the two rosettes can be linked on the one hand to the quality and resolution of the photographs which did not make it possible to map the fractures properly and on the other hand to the absence of techniques improvement of images at the level of photography acquired only in the visible. However, in a modeling approach, fitting a normal distribution per family would be acceptable. In short, it should be noted here that the major lineaments present a great heterogeneity in their orientation, with a preponderance and will be considered as fractures The difference in fracturing density recorded at the level of the two rosettes can be linked on the one hand to the quality and resolution of the photographs which did not make it possible to map the fractures properly and on the other hand to the absence of techniques improvement of images at the level of photography acquired only in the visible. However, in a modeling approach, fitting a normal distribution per family would be acceptable. In short, it should be noted here that the major lineaments present a great heterogeneity in their orientation, with a preponderance and will be considered as fractures The difference in fracturing density recorded at the level of the two rosettes can be linked on the one hand to the quality and resolution of the photographs which did not make it possible to map the fractures properly and on the other hand to the absence of techniques improvement of images at the level of photography acquired only in the visible. However, in a modeling approach, fitting a normal distribution per family would be acceptable. In short, it should be noted here that the major lineaments present a great heterogeneity in their orientation, with a preponderance and will be considered as fractures [56].

3.2.2. Validation of the Lineament Map by Overlaying Boreholes

- **Positive drilling positioning**

It is applied to all the directions of the lineaments as shown in Figure 7. In this sense, to validate the lineaments in fractures, we propose to study the relations between direction of orientation and distance. For a total of 146 boreholes, we note that 60 boreholes or 41.10% of the boreholes correspond to the different intersections of the lineaments, which suggests that this is consistent with the fractures in the basement. Subsequently, we see that the remaining 86 boreholes, i.e. 58.90%, do not overlap on the images. Insofar as a borehole can capture several directions, the percentage of impacted boreholes according to the orientations are as follows: the NO-SE direction is exploited by 11 boreholes, i.e. 18.33% the NE-SW direction is exploited by 39 boreholes, i.e. 65.00%, the NS direction is exploited by 11 boreholes, i.e. 11.67%, the EW direction is exploited by 3 boreholes, i.e. 5.00%. This can be explained by the fact that some boreholes capture secondary lineaments which are poorly known. The analysis of the different percentages makes it possible to classify the lineaments according to their influence in the positioning of the boreholes: NE-SW > NO-SE > EW > NS. The predominant directions and the preferential directions of lineaments oriented N60°-70°, N100°-115° and N120°-130° (NE-SO) and (NO-SE) are the most represented, then the N10° directions -20° (NS) follow. Similar results by a dominance of NO-SE directions have been obtained by different authors [58,59,60,61] in the same base environment and which describe that there is a low percentage of correlation on the directions. The intensities of dominant lineaments correspond mainly to the domains of schists, granite and magmatic granites which results from a tectonic activity giving rise to a hydrographic network. On a large scale, directions with a high local density appear, whereas on a regional level they are at a low frequency rate. The superimposition also gives us information on open joints, in directions N90°-N100°, N120°-N130° and N160°. It was retained that the open directions are the most capable of playing a drainage role with respect to the surrounding alterites [19].

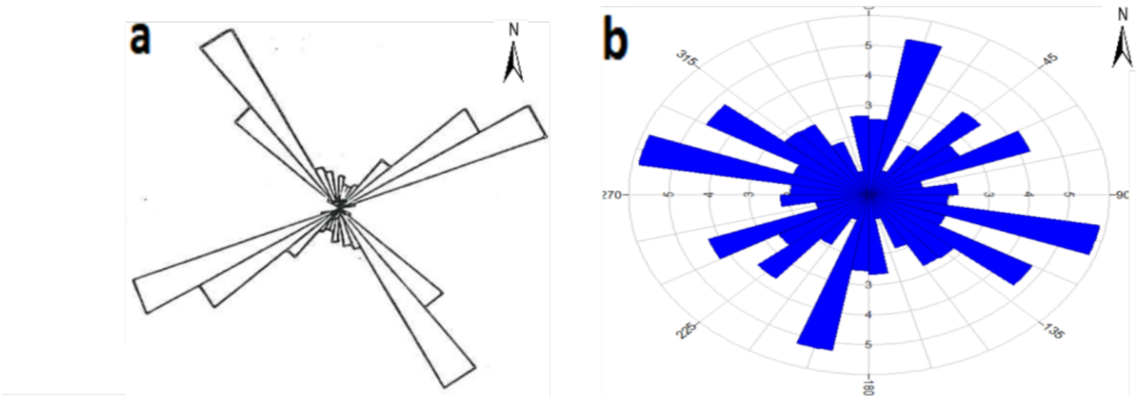

Figure 6. a) Aerial photography rosette b) Landsat rosette

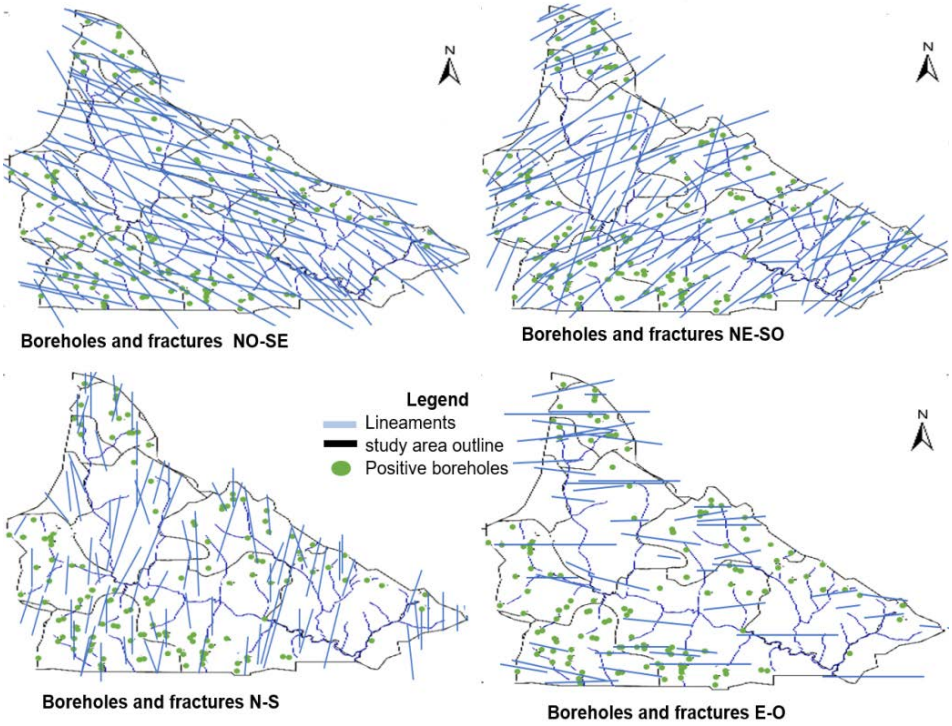

Figure 7. Superposition of positive boreholes in relation to the orientations of the lineaments of the Sissili sub-basin

- **Positioning negative boreholes**

For the 60 negative boreholes as illustrated in Figure 8, it is noted that the direction captured mainly in line with the boreholes is the NS direction. Indeed, out of 60 boreholes concerned, 27 boreholes are NS directions, i.e. 45.00% of the negative boreholes: the NO-SE direction is exploited by 14 boreholes, i.e. 23.33%, the NE-SW direction is exploited by 15 boreholes, i.e. 25.00%, the NS direction is exploited by 26 boreholes, i.e. 43.33%, the EW direction is exploited by 5 boreholes, i.e. 8.33%. This confirms following the superposition of several directions, that some directions can have closed joints (NS) N0°-N10°, but also the directions (EO) N60°-N80°. Indeed, the observation on the ground and the data collected on the negative drillings confirm that the direction can play on the nature of the joint.

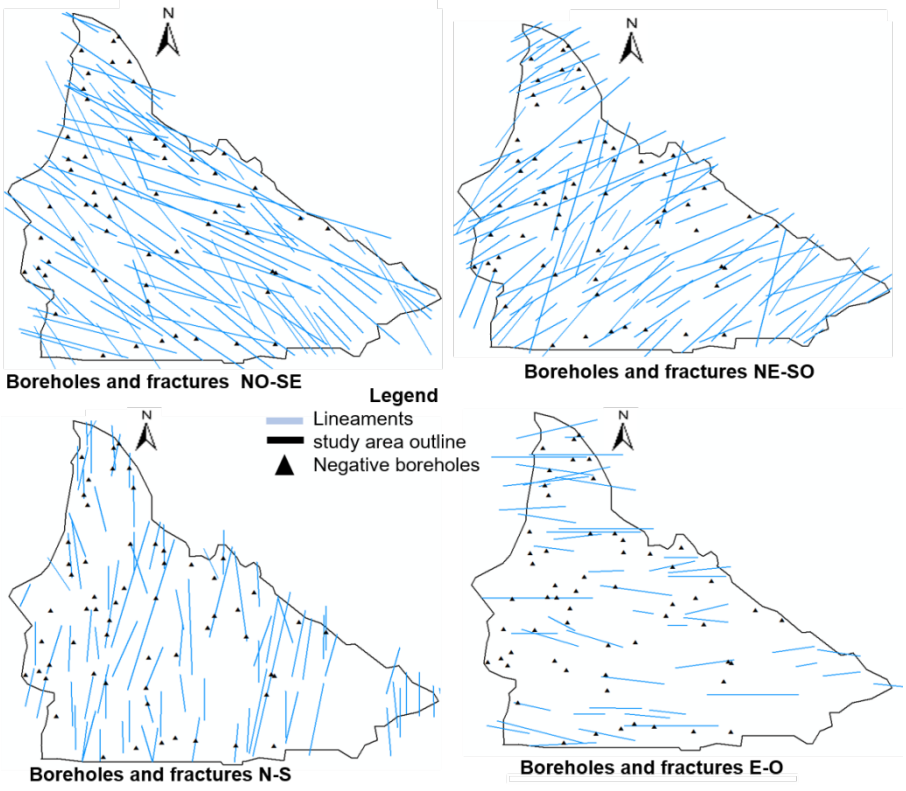

Figure 8. Superposition of negative boreholes in relation to the orientations of the lineaments of the Sissili sub-basin

• **Separation distances**

Subsequently, the distance of each borehole from the lineaments was measured. The percentage of positive and negative boreholes impacted according to the orientations is represented by Figure 9 and listed in Table 2. According to the results, the implantation of boreholes in the sub-basin was most often done by trial and error. Figure 9b shows us a peak of 93.33% at the level of negative boreholes and 38.36% for positive boreholes at 200 meters distance.

Table 2. Percentage of boreholes following all orientations

	Distance	[0−200]	[200-400]	[400−600]	[600-800]	[800−1000]	[1000−1200]	[1200−1400]
	Number	10	56	91	120	128	133	136
F. Positive	%	6.85	38.36	62.33	82.19	87.67	91.1	93.15
F. Negative	%	61.67	93.33	80	88.33	93.33	96.67	100

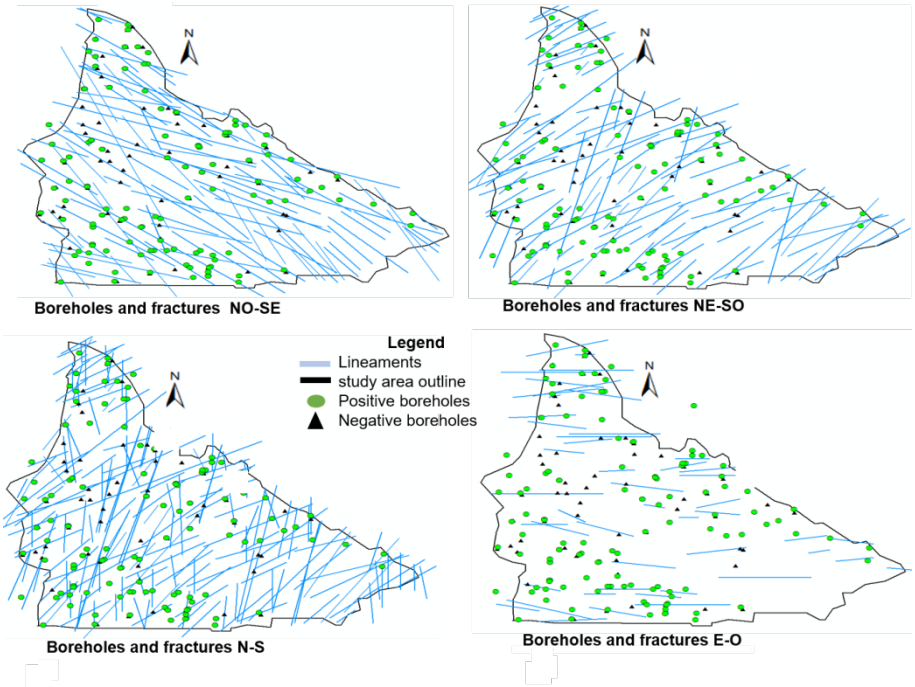

Figure 9a. Distance of each borehole from the lineaments

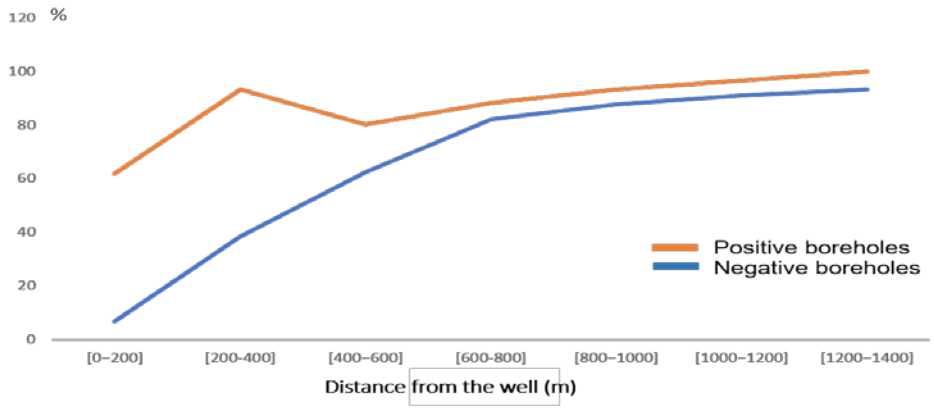

Figure 9b. Distance of each borehole from the lineaments

Table 3. flow classification

CIEH flow class	Number	%
[0−1] Very low	49	38.58 NW-SE
[1−2.5] Low	34	26.77 NW-SE
[2.5−5] Means	21	16.54 NE-SW
[>5] Strong	23	18.11 NE-SW
Total	127	100

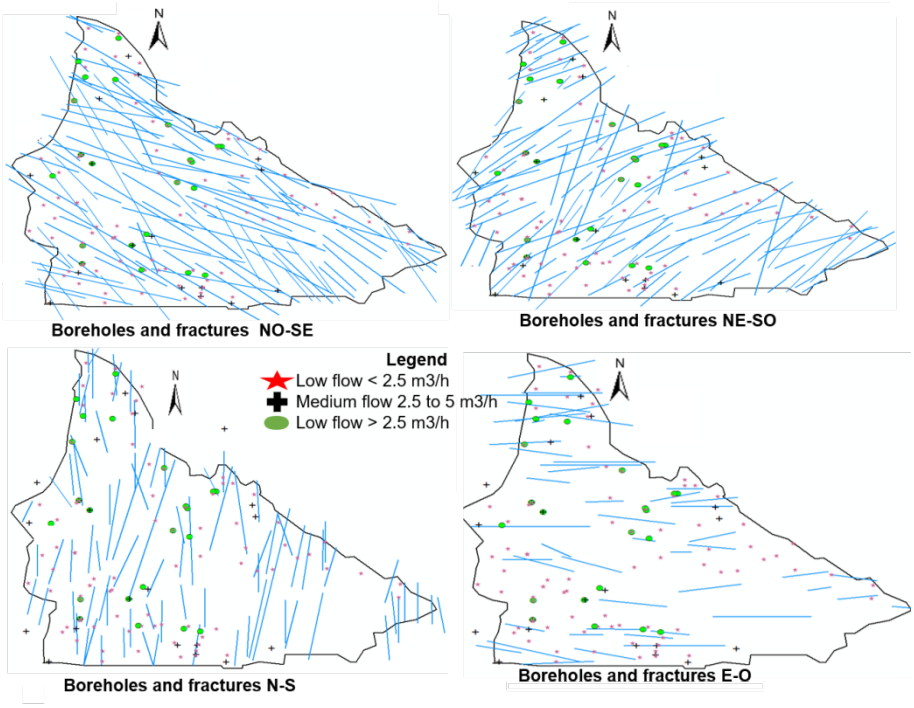

Figure 10. Relationship between flow class and fracture orientations

- **Flow class**

The study of flow classes in relation to lineaments and directions of fractures NS, EO, NE-SW and NO-SE was carried out and represented by Figure 10. Among the 146 boreholes, only 127 boreholes have flow rates varying from 0.04 m^3/h at Taré to 18 m^3/h at Boala and are concerned by this study. Flow classes greater than 5 m^3/h are observed in granite zones with "V" and "U" anomaly shapes, but the "W" shape has the highest success rate. The highest discharges correspond to type "H" curves, followed by type "A". In terms of productivity, granite formations are the most productive. However, all orientations are likely to provide low discharge. Table 3 represents the classification of flows according to the [24,63,64]. The analysis shows us that 65.35% of the low flows are lower than 2.5 m^3/h. This rate is certainly due to the fact that these boreholes capture or are positioned on the secondary lineaments. This may also be due to the fact that the locations of these boreholes have not been the subject of an in-depth study and should above all be close to dwellings. The lowest flows in the area are observed in the directions of fractures harboring the NW-SE direction. The zone with a strong structural trend identified by remote sensing certainly corresponds to an underground corridor which is expressed by small fractures, but in large numbers as in the case of Koukin and Thiakané. The remaining 34.65% of boreholes have flow rates greater than 2.5 m^3/h; which suggests that these boreholes were the subject of a lineament mapping study followed by validation by geophysics. The best flows in the area are observed in the directions of fractures sheltering the NE-SW direction.

- **Flow classes and depth**

The relationship between the flow classes and the depth of the structures (Figure 11) gives an average of 58.3 meters. The greatest depth is observed at 86 meters in the locality of Nation and the smallest of 37 meters in the locality of Kombila. Figure 11 illustrates that low flows are found at all depths, while high flows are between 43 meters to 84.75 meters distributed in the 3 provinces and medium to high flows are between depths 45 meters 80 meters away. This high throughput productivity confirms the study of [48] which describes that the limit of occurrence of open joint fractures is between 30 and 60 meters, whereas [61] sets this limit between 50 and 70 meters. This analysis confirms that the depth of the boreholes does not necessarily guarantee high flows, for example in the locality of Sapouy for 3 boreholes of respective depths of 74 m, we have flows of 10 m^3/h, 6.14 m^3/h and 0.60 m^3/h. This supposes that at great depths there can be the presence of a productive fracture.

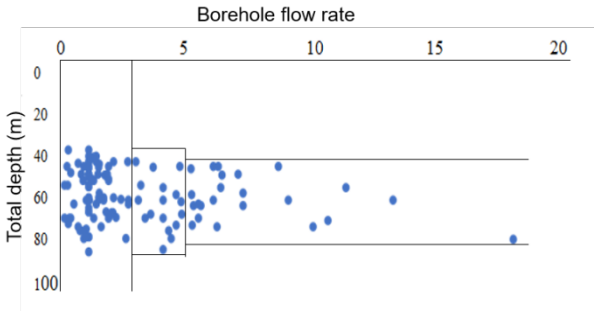

Figure 11. Relationship between flow rates and total borehole depth

- **Flow classes and alteration thicknesses**

The relationship between flow classes and alteration thicknesses (Figure 12) shows that between the depths of 12.94 to 40.31 meters, the highest flows are recorded with an influence on the thicknesses. Low flows are noticeable below 12.94 meters and above 40.31 meters thick. These results are similar to those of [65] which explains that this result is linked to an accumulation of water from alterites through drainage phenomena. Then, the strongest thicknesses at low flow reveal that the drainage is obstructed while the weakest thicknesses describe that the holding capacity is biased and that the aquifer is subject to

seasonal fluctuation. In addition, the load tends to compress cracks as the depth increases. The leaching of materials altered by infiltration can also partially seal the cracks. In this case, the top of the fractured zone is expected to have hydraulic parameters close to those of the arenas above it.

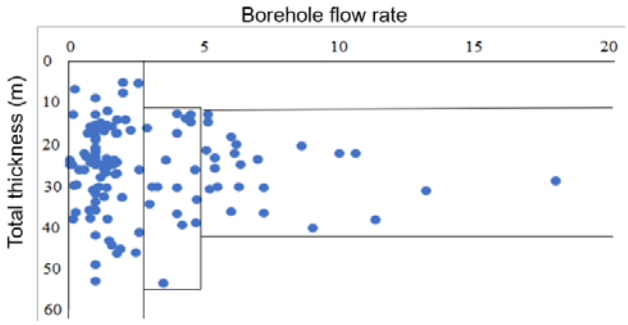

Figure 12. Relationship between flows and weathering thicknesses

3.3. Validation of the Linear Map by Geophysical Investigations

3.3.1. Case of Electric Trails

The interpretation of the 12 trails carried out reveals discontinuity zones whose characteristics are represented in Table 4. The determination of their directional orientations by the parallel profiles obtained by geophysics, made it possible to validate the lineaments which alter the sound rock in fractures. These are usually represented by areas of low resistivity. The validation of the lineaments in the villages of Kada and Sissili Mossi showed other lineaments which could not be perceived at the level of the satellite images. The drag profiles implanted tell us about high (hard rock) to low (associated with high permeability fractures) resistivity and the shape of the anomalies. The main profile meets a peak at the location of the existing borehole. The drag profile carried out in the villages of Koukin and Tiakané shows that the anomalies encountered give the best results, whatever the geological context. The identification of discontinuity zones and their orientations allowed us to map the fractures that alter the sound rock. The parallel profiles on the same graph make it possible to highlight the extension and the orientation of these discontinuities materialized by alignments of conductive anomalies. This is the case of the variation where the bedrock is covered with highly conductive clay veneer. The profiles show less contrasting values on the granites or migmatites. The lineaments located by the satellite images favor a greater extension of the zone of influence, and often a single drag profile is sufficient for the implantation of the boreholes. But if the required speeds are high, many profiles are studied. There is therefore a vast zone of resistivity varying from 200 to 400 Ω.m and direction N° 156 N°180 at Kada, N°146 N°190 N°142 at Sissili Mossi, N°212 N°174 at Koukin, and No. 145 No. 149 No. 202 in Tiakané. The thicknesses of the zone vary from 20 m to 50 m and are a probable index of the intense fracturing that has occurred in the sub-watershed. The impact of the change in depth of investigation on their pace highlighted several discontinuities or fractures favorable to the implantation of boreholes. In effect [66] and [67], show that the shape of the anomaly determines the success rate. It is therefore important to take into account the shape of the anomaly highlighted on the resistivity profile for the drilling locations. These levels correspond in our case to 6 varied forms of anomaly (“V” at 30%,”U” at 10%,”W” at 8.9%,”H” at 6.8%, the “M” forms, and “ K” are not taken into account, because they are insignificant) and are most often associated with zones of discontinuities. We have a higher rate with anomalies in “W and V” shapes which are associated with NE-SW directions on the granites. Indeed, it is considered that the anomalies of “V” shapes are linked to minor fractures settling on either side of a major accident and those of the “W” shape are linked to parallel fractures. On the other hand, 19% of failed boreholes are “U” shaped. The results of our study confirm those of the work of [68] in a basement environment in Burkina with the use of this prospecting method. The most recommended method is the one with the Schlumberger drag profile device. We can observe on the different drag profiles that in some areas, the fractures are of low extension or they may be discontinuous pockets of water separated by sills. The studies of [69] on the analysis of productivity and those of [64] on water search methods show us that a fracture parallel to the tectonics is open while those that are orthogonal are closed. The study of [30] in the same basement environment confirms these same results. In the village of Sissili Mossi, we observed negative boreholes on the same drag profile, because most of them are in the NW direction which according to [70] is waterproof. We can therefore conclude that the NE and SO directions are productive while the NO and SE directions are tight in our sub-basin as shown in Figure 13a for the main profiles and Figure 13b for the paralleling profiles.

Table 4. Representation of electrical profile characteristics

Site	Koukin	kada	Sissili Mossi	Tiakane
Distance	860	400	400	400
AB/2	200	200	200	200
MN	10	10	10	10
Direction	N° 90	N° 70	N° 70	N° 90
Observed resistivity (Ω.m)	261	280	340	203
Thickness (m)	18	20		
Type of anomaly	U&H&K	V	V	W
Direction of lineaments	N° 212 & 174	N° 156 & 180	N° 146 & 190 & 142	N° 145 & 149 & 202

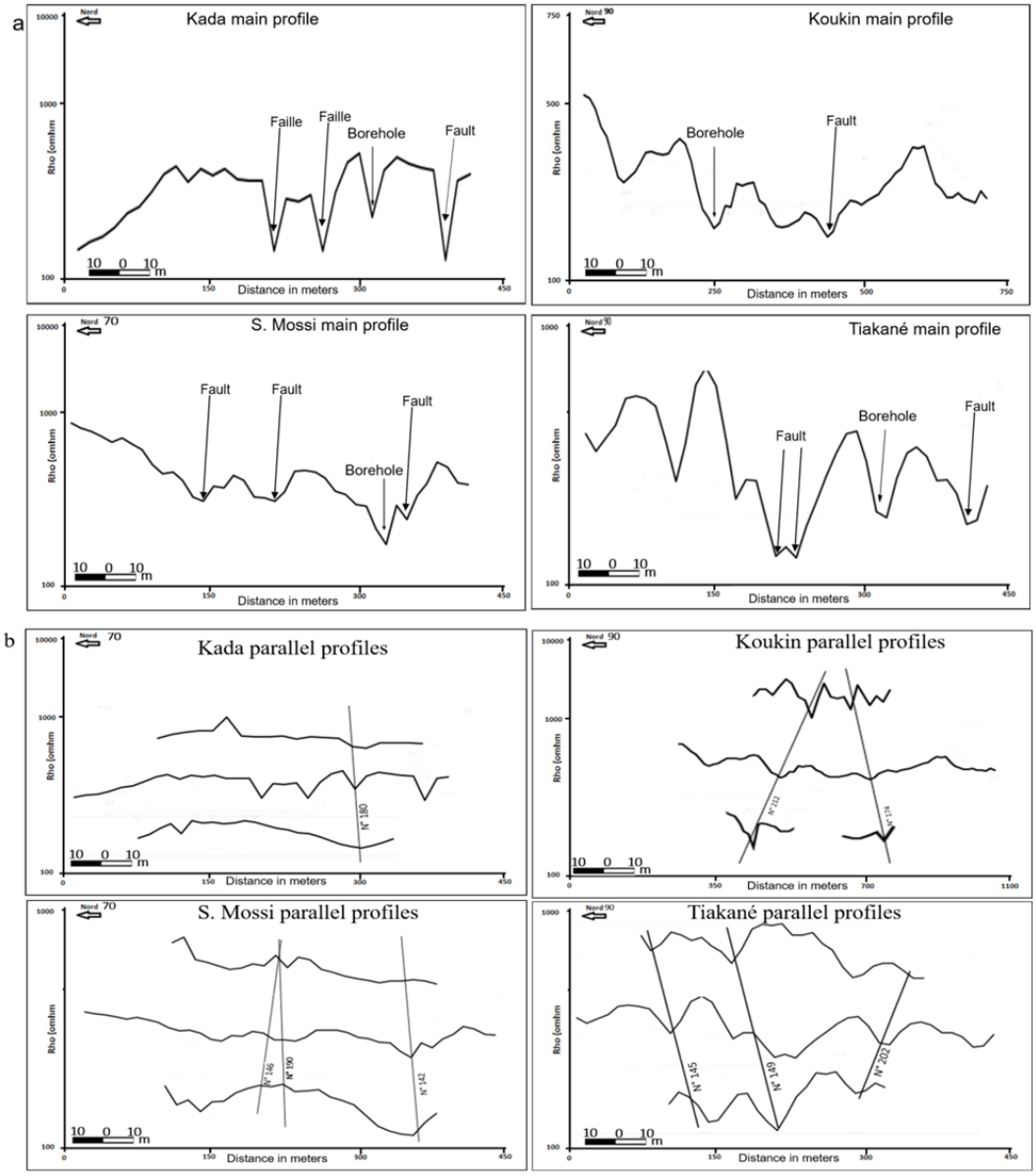

Figure 13. Fractures recognized from the main profile and three parallel profiles

3.3.2. Case of Electrical Soundings

The surveys carried out as part of this study give us three (3) types of curves, namely the "H" type at 40%, the "A" type at 35%, and finally the "KH" 25%. These curves, which have different shapes, are representative of the conceptual models of the basement formations. Indeed, the basement formations can be represented by a vertical profile composed of three layers including Saprolite (Alloterite [17m to 20m] and Isalterite [19m to 22m]), fissured source rock (18m to 20m) and rock healthy mother (6m to 10m).

A gait at the bottom of the boat of the "H" curve type designates a conductive formation made up of granite, and whose fracture is not materialized. It does not give any indication of the cracked zone due to its low thickness at great depths. This is the case of SE3 Koukin Figure 14a ($\rho1 > \rho2 < \rho3$) which generally characterizes regions with superficial lateritic armour. This type of curve is most often characterized by a 45° rise at the level of the sound substratum corresponding to three layers. In many cases, the resistivity of the cuirass is lower compared to arenas with variegated clays. However, if one faces two layers of layers formed at the level of the drowned cuirass and the arenas, the curve becomes a five-layer curve. The conductive enclosures point to the boat bottom of the curve. They are composed of fluent clayey quarries and fissured rock which, when thin, goes unnoticed on the sounding curve. This is why the true resistivity are difficult to calculate especially when they are not very powerful. On granite rocks, a high permanent humidity of clayey alterites makes them very conductive even though they do not contain usable water. Very low resistivity is then obtained which, despite the high resistivity of the armour, give a boat bottom. There is a good correlation between the curve and the field data on shales than on granites where the resistivities are generally high. This allows us to say that in a shale zone, whatever the type of sounding, the success rate is relatively high compared to that in the granite zone. The thicknesses of alterations of the order of 20 m to 30 m seem the most favorable, whatever the nature of the geological formation [23,66,71].

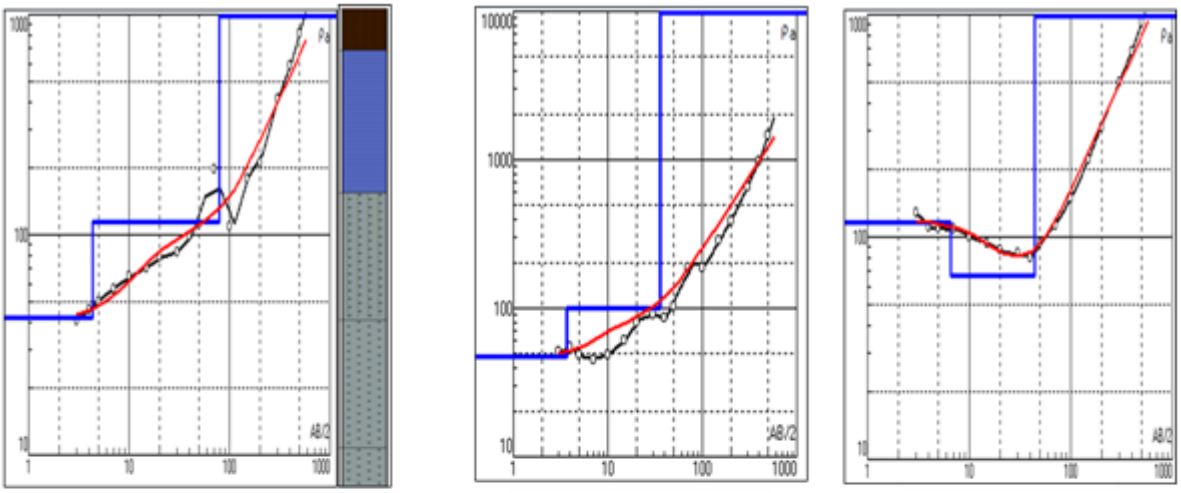

a) Electrical sounding profiles of the Commune of Thyou: village of Koukin

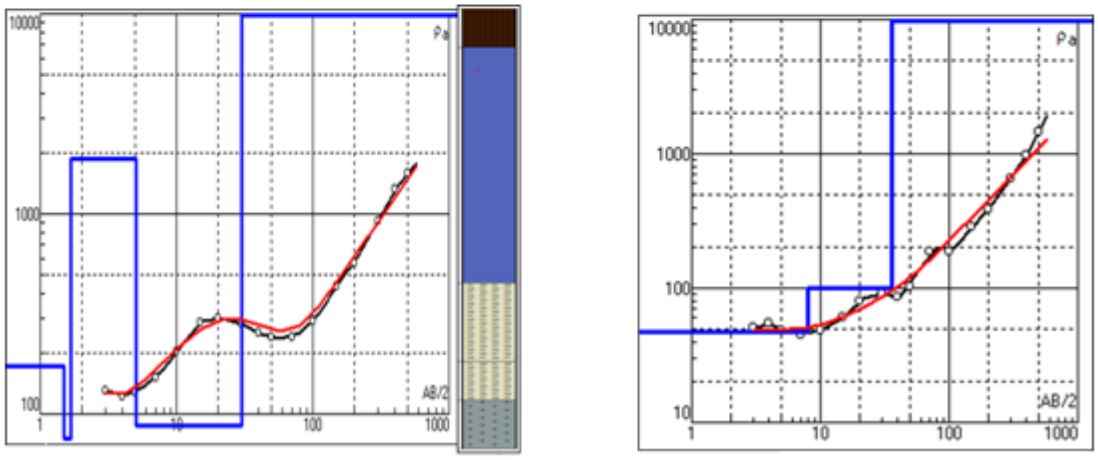

b) Electrical sounding profiles of the Municipality of Sapouy: village of Kada

Figure 14. Electrical wave of the Municipality of Thyou and Sapouy

Boreholes SE1 and SE2 at Koukin Figure 14a and SE2 Kada Figure 14b present a pattern with a single rising branch of type A corresponding to two layers with a small slope. The first layer corresponds to a horizon of conductive arenas with variations in clay, laterite or water content. The second layer corresponds to the resistant substratum which constitutes the altered or fissured horizon and highlights a strong alteration especially in the schistous domain which is more conductive. This type of sounding is related to the influence of a mega fracture. It should also be remembered that a conductive anomaly can produce negative boreholes. The study of the ground layers shows an inconsistency especially at the level of the SE1 drilling of Koukin Figure 14a. The drilling cross-section gives 5 layers of land while the sounding profile gives 3 layers of land knowing that the shape of the sounding curves is at the origin of the difference observed in the number of layers. This can be explained by the fact that at the level of the sounding, the change in slope does not necessarily correspond to changes in terrain. Rather, they correspond to variations in water content in the same layer. In addition, two layers on the drilling log are identified as being a single layer at the borehole level. By summing the thicknesses of the terrains in question on the log, we obtain the thickness of the layer identified with the sounding. These results are similar to those of Rather, they correspond to variations in water content in the same layer. In addition, two layers on the drilling log are identified as being a single layer at the borehole level. By summing the thicknesses of the terrains in question on the log, we obtain the thickness of the layer identified with the sounding. These results are similar to those of Rather, they correspond to variations in water content in the same layer. These results are similar to those of [72]. They explain this phenomenon by the fact that the layers have almost identical resistivities; which does not facilitate the observation on the sounding curve of a change in slope which would mark a change in terrain. Indeed, the only rising branch can be productive if the supply is good as in the case of coarse tectonized granites or lowland areas.

The SE1 Kada sounding in Figure 14b presents a bell shape then a KH-type boat bottom corresponding to four layers. The first layer corresponds to the superficial terrain with resistivities of 172 Ω.m and a low thickness of 1.5 m. The second layer corresponds to the conductive arenas which are split into 2 layers. And finally we observe a resistant substratum corresponding to the fissured horizon [19]. Another scenario with a similar appearance is when the thick ferruginous armour is dismantled (reworking by a termite mound, quarrying). It should also be noted that

on SE2 at Kada Figure 14a, the lateritic cuirass is compact and influences the curve by a vertical translation over the entire curve. In this case, the sounding curve is presented in curves of 3 plots; which gives low values to the streaks while the covering thickness is low. Resistivity values are lower on schists and sedimentary volcanic rocks than on granites and migmatites; which is due to the clay content. At the level of the migmatite granites, micro-fractures are observed which favor a greater extension of the zone of influence. Indeed, when the profile intersects the fracture to be validated, it is the intersection which is most often known with precision. The direction of the axis rarely is, as it is determined interpretively.

In general, the failure rate of boreholes in the Sissili sub-basin can be attributed to geophysical prospecting methods or to several phenomena related to the subsoil during implantation. These failures are related to a conductive anomaly due to a superficial phenomenon. Indeed, some anomalies may be due to variations in resistivity of the surface covering unrelated to fracturing. This is the case of the presence of a thick layer of waterlogged clay in the low resistivity alterites which is similar to a fissured rock. To remedy this, [72] offers resistivity profiles with a square device especially in crystalline medium. Other authors define these failures by the fact that the fracture can be inclined according to the direction of the flow from which the water accumulates in depth. The fracture defined by the electric sounding can also be sterile or mineralized with very low water content. These authors give priority in hydrogeological prospecting of crystalline and crystallophyllian basement to sounding curves at the bottom of the boat. This difference is explained by the fact that the choice of sites does not take into account the combination of indicators of types of forms of anomalies and types of soundings.

However, the practice of this method (1D) remains. Indeed, the (1D) probing technique has well-known advantages and limits. Its implementation comes after that of the trailing profile which makes it possible to identify the discontinuity to be intersected. The major difficulty lies in the presence of greenery and cultivable area which do not facilitate a good characterization of the geometry of the aquifer (1D). It tends to group the layers of the drilling log into a single layer which underestimates the thickness as in the case of the Koukin drilling.

The trailing (1D) technique has its limitations, as trails are interpreted based on apparent resistivities [21], or based on the width and shape of the discontinuity [66]. But the profile analysis reveals that the zone containing lateritic clay presents very surprising structures in terms of diversity, sometimes superior to that of the discontinuity structures of the fissured zone. To this we can add that the method used as the Schlumberger can lead to discrepancies. Indeed, this is confirmed by the results of the synthetic modeling which concludes that the Wenner device is more suitable and produces less deviation [16]. However, it has limitations in estimating the depth of fissured zones and its implementation. [21] shows that regardless of the dragging method implemented, the discontinuities sub verticals in the unweathered zone cannot be determined.

4. Conclusions

The advent of satellite images these days constitutes a powerful tool for groundwater exploration. The processing and analysis of Landsat 8 images has contributed to the mapping of poorly known fracture networks in our sub-basin. The fracturing map taken from satellite imagery must necessarily be coupled with hydrogeological data through a GIS for a better exploitation of water resources. The Sissili sub-basin appears to us to be a very favorable zone for the installation of boreholes. Nevertheless, it has areas where negative boreholes or low flows are recorded. Depending on the method used, the results show us preferential fracture directions N15°, N60° and N120°. We also determined the NE and NS directions as productive and the NW and EW directions as tight. The conclusions of the geophysical prospection by the trailed show us anomalies of form U, V, and K. The parallel profiles give us directions N° 156 N°180 in Kada, N°146 N°190 N°142 in Sissili Mossi, N°212 N°174 in Koukin, N°145 N°149 N°202 in Tiakané. The soundings give us three forms A, H and KH with different productivities. The dissimilarities at the level of the layers and thicknesses are the probable causes of many failures during the implantation of the boreholes. The drilling conclusions confirm those obtained by the data from the geophysical surveys. The electrical investigations (1D) and the statistical analysis of the drilling data allowed us to understand and justify the failures of the drillings due to the absence of resemblance at the level of the layers, the characteristics of the alteration and the direction of the fracture. In the rest of this work, these results will be coupled with hydrodynamic data to optimize the failure rate of the boreholes. The association of this study with that of underground flow through numerical modeling would be interesting.

References

[1] N. Courtois *et al.*, "Large-Scale Mapping of Hard-Rock Aquifer Properties Applied to Burkina Faso," *Ground Water*, vol. 48, no. 2, pp. 269-283, Mar. 2010.

[2] A. Sako, O. Bamba, and A. Gordio, "Hydrogeochemical processes controlling groundwater quality around Bomboré gold mineralized zone, Central Burkina Faso," *Journal of Geochemical Exploration*, vol. 170, pp. 58-71, Nov. 2016.

[3] M. D. Faye, M. B. Kafando, B. Sawadogo, R. Panga, S. Ouédraogo, and H. Yacouba, "Groundwater Characteristics and Quality in the Cascades Region of Burkina Faso," *Resources*, vol. 11, no. 7, p. 61, 2022.

[4] D. D. Moghaddam *et al.*, "The effect of sample size on different machine learning models for groundwater potential mapping in mountain bedrock aquifers," *Catena*, vol. 187, p. 104421, 2020.

[5] B. Valfrey-Visser and M. Rama, "Rapport pays- Etats des lieux de l'eau et de l'assainissement au niveau national, Livre Bleu BURKINA FASO, deuxième édition." 2012.

[6] R. C. Carter and A. Parker, "Climate change, population trends and groundwater in Africa," *Hydrological Sciences Journal*, vol. 54, pp. 676-689, 2009.

[7] B. Choubin, O. Rahmati, F. Soleimani, H. Alilou, E. Moradi, and N. Alamdari, "Regional groundwater potential analysis using classification and regression trees," in *Spatial modeling in GIS and R for earth and environmental sciences*, Elsevier, 2019, pp. 485-498.

[8] L. Karimi, M. Motagh, and I. Entezam, "Modeling groundwater level fluctuations in Tehran aquifer: results from a 3D unconfined

aquifer model," *Groundwater for Sustainable Development*, vol. 8, pp. 439-449, 2019.

[9] J.-E. Paturel, I. Boubacar, A. l'Aour, and G. Mahé, "Analyses de grilles pluviométriques et principaux traits des changements survenus au 20ème siècle en Afrique de l'Ouest et Centrale," *Hydrological Sciences Journal–Journal des Sciences Hydrologiques*, vol. 55, no. 8, Art. no. 8, 2010.

[10] S. Y. Rathay, D. M. Allen, and D. Kirste, "Response of a fractured bedrock aquifer to recharge from heavy rainfall events," *Journal of Hydrology*, vol. 561, pp. 1048-1062, 2018.

[11] N. Savadogo, "Hydrogéologie du bassin versant de la Haute-Sissili (Haute-Volta)," octoral dissertation, Université scientifique et médicale de Grenoble, France, 106 p, 1975.

[12] M. D. Faye, A. C. Biaou, D. D. Soro, B. Leye, M. Koita, and H. Yacouba, "Understanding groundwater pollution of sissili catchment area in BURKINA-FASO," *LARHYSS Journal P-ISSN 1112-3680 / E-ISSN 2521-9782*, vol. 0, no. 42, Art. no. 42, Jul. 2020.

[13] G. Ewodo Mboudou, A. F. Bon, E. Bineli, F. Ntep, and A. Ombolo, "Caracterisation de la productivite des aquiferes du socle de la region de l'extreme Nord, Cameroun," Journal of the Cameroon Academy of Sciences, vol. 14, no. 1, p. 25, Jan. 2018.

[14] Y. Koussoube, "Champs captants sur mégafractures du socle et généralisation des réseaux d'adduction d'eau potable en milieu rural: concept et faisabilité technique", *Rév. Ivoir. Sci. Technol*., 30, 235-251, 2017.

[15] P. Lachassagne, R. Wyns, and B. Dewandel, "The fracture permeability of Hard Rock Aquifers is due neither to tectonics, nor to unloading, but to weathering processes: Weathering and permeability of Hard Rock Aquifers," *Terra Nova*, vol. 23, no. 3, pp. 145-161, Jun. 2011.

[16] D. D. Soro, "Caractérisation et modélisation hydrogéologique d'un aquifère en milieu de socle fracturé: cas du site expérimental de Sanon (région du plateau central au Burkina Faso)," Thése de doctorat, Université Pierre et Marie Curie-Paris VI, France, Institut international d'ingénierie de l'eau et de l'environnement, Burkina Faso, 304 p, 2017.

[17] H. Karambiri *et al.*, "Assessing the impact of climate variability and climate change on runoff in West Africa: the case of Senegal and Nakambe River basins," *Atmospheric Science Letters*, vol. 12, no. 1, pp. 109-115, 2011.

[18] G. Giot and M. Seger, "Un dispositif pédagogique de mesure de la résistivité électrique: Illustrer par l'expérience l'apport des méthodes géophysiques pour la caractérisation des propriétés du sol," *Etude et Gestion des Sols*, vol. 26, pp. 125-131, 2019.

[19] N. Savadogo, "Géologie et hydrogéologie du socle cristallin de Haute-Volta: Etude régionale du bassin versant de la Sissili," Doctoral dissertation, Université scientifique et médicale de Grenoble, France, 180 p, 1984.

[20] A. Samouëlian, I. Cousin, A. Tabbagh, A. Bruand, and G. Richard, "Electrical resistivity survey in soil science: a review," *Soil and Tillage research*, vol. 83, no. 2, pp. 173-193, 2005.

[21] I. C. Alle, "Évaluation de l'implantation géophysique des forages d'eau en zone de socle en milieu tropical (Bénin, Afrique de l'Ouest): apport de la tomographie de résistivité électrique pour la caractérisation de la cible hydrogéologique," PhD Thesis, Université d'Abomey-Calavi (Bénin), 2019.

[22] A. Yameogo, Y. S. C. Some, A. B. Sirima, and D. E. C. Da, "Occupation des terres et érosion des sols dans le bassin versant supérieur de la Sissili, Burkina Faso," *Afrique Science*, vol. 17, no. 5, Art. no. 5, 2020.

[23] N. Savadogo, "Hydrogéologie du bassin versant de la Haute-Sissili (Haute-Volta," (PhD Thesis)., 1975.

[24] D. Giovenazzo et al., "Notice explicative de la carte de synthèse géologique, structurale et des substances minérales du BURKINA FASO à l'échelle 1/1 000 000", L'équipe d'Effigis Géo-Solutions. 2018.

[25] R. Dahl, et al., "*Carte de synthèse géologique, structurale et des substances minérales du BURKINA FASO à l'échelle 1/1 000 000"*, Effigis Géo-Solutions. 2018.

[26] M. Y. Ta *et al.*, "Apport de la Cartographie Lithostructurale par Imagerie Satellitaire Landsat 7 à la Connaissance des Aquifères du Socle Précambrien de la Région de Bondoukou (Nord-Est de la Côte D'ivoire)/[Contribution of the Lithostructural Mapping By Landsat 7 Imagery To Study the Precambrian Basement Aquifers in Bondoukou Region (Northeast Coast Ivory," *International Journal of Innovation and Applied Studies*, vol. 7, p. 892, 2014.

[27] Y. Nicaise, A. H. Bertrand, Y. T. Marc, and A. George, "Apport De La Télédétection Et De La Géophysique Dans La Cartographie Des Fractures Hydrauliquement Actives En Zone De Socle Au Centre-Ouest Du Benin." 2019.

[28] P. Li, L. Jiang, and Z. Feng, "Cross-Comparison of Vegetation Indices Derived from Landsat-7 Enhanced Thematic Mapper Plus (ETM+) and Landsat-8 Operational Land Imager (OLI) Sensors," *Remote Sensing*, vol. 6, pp. 310-329, 2013.

[29] Z. Adiri *et al.*, "Comparison of Landsat-8, ASTER and Sentinel 1 satellite remote sensing data in automatic lineaments extraction: A case study of Sidi Flah-Bouskour inlier," *Moroccan Anti Atlas. Advances in Space Research*, vol. 60, pp. 2355-2367, 2017.

[30] A. P. Sombo, K. É.-G. Kouakou, S. G. Eblin, and B. C. Sombo, "Caractérisation hydrogéologique, par télédétection et géophysique d'accidents régionaux en zone de socle: cas de Sikensi-Tiassalé, Côte d'Ivoire," *Afrique SCIENCE*, vol. 15, pp. 313-327, 2019.

[31] H. Kabanyegeye, Y. Useni Sikuzani, K. R. Sambieni, T. Masharabu, F. Havyarimana, and J. Bogaert, "Trente-trois ans de dynamique spatiale de l'occupation du sol de la ville de Bujumbura, République du Burundi," *Afrique Science: Revue Internationale des Sciences et Technologie*, vol. 18, no. 1, 2021.

[32] K. S. Dahan and K. C. N'DA Dh assi, "Dynamique spatiotemporelle des feux de 2001 à 2019 et dégradation du couvert végétal en zone de contact forêt-savane, Département de Toumodi, Centre de la Côte d'Ivoire," *Afrique SCIENCE*, vol. 19, no. 2, pp. 94-113, 2021.

[33] B. Jaziri, "Analyse cartographique et paysagère des transformations spatiales du couvert forestier des Mogods (Tunisie septentrionale)," *Physio-Géo. Géographie physique et environnement*, no. Volume 15, pp. 1-27, 2020.

[34] A. T. Tran, K. A. Nguyen, Y. A. Liou, M. H. Le, V. T. Vu, and D. D. Nguyen, "Classification and observed seasonal phenology of broadleaf deciduous forests in a tropical region by using multitemporal sentinel-1a and landsat 8 data," *Forests*, vol. 12, no. 2, p. 235, 2021.

[35] P. Ghimire, D. Lei, and N. Juan, "Effect of image fusion on vegetation index quality—a comparative study from Gaofen-1, Gaofen-2, Gaofen-4, Landsat-8 OLI and MODIS Imagery," *Remote Sensing*, vol. 12, no. 10, p. 1550, 2020.

[36] A. Cerbelaud *et al.*, "Potentiel de l'imagerie optique satellitaire à haute résolution pour détecter les dommages engendrés par des épisodes pluvieux extrêmes☆," *La Houille Blanche*, 2021.

[37] F. Jedrzejewski, "14 Traitement de l'image," in *Mathématiques pour l'imagerie médicale*, EDP Sciences, 2021, pp. 207-216.

[38] G. Ouattara and G. B. Koffi, "Contribution des images satellitales Landsat 7 ETM+ à la cartographie lithostructurale du Centre-Est de la Cote d'Ivoire (Afrique de l'Ouest)," *International Journal of Innovation and Applied Studies*, vol. 1, no. 1, pp. 61-75, 2012.

[39] K. F. Kouamé, T. Lasm, M. B. Saley, E. Tonyé, M. Bernier, and S. Wade, "Extraction linéamentaire par morphologie mathématique sur une image RSO de RadarSat-1: application au socle Archéen de la Côte d'Ivoire," *IIIèmes Journées d'Animation Scientifique du réseau de Télédétection de l'AUF JAS'09, Sous le thème:«Imagerie Satellitaire Multisources: Approches Méthodologiques et Applications*, 2009.

[40] E. Onat, "FPGA implementation of real time video signal processing using Sobel, Robert, Prewitt and Laplacian filters," in *2017 25th Signal Processing and Communications Applications Conference (SIU)*, IEEE, 2017, pp. 1-4.

[41] G. L. Shungu, "Etude Structurale des formations de l'Ouest du lac Tanganyika (cas de Kavimvira, RD Congo)," *International Journal of Innovation and Applied Studies*, vol. 24, no. 1, pp. 299-310, 2018.

[42] T. Miyouna, B. T. NC, O. F. Essouli, A. Kempena, H. M. D.-V. Nkodia, and F. Boudzoumou, "Cartographie par traitement d'image satellitaire des linéaments du groupe de l'Inkisi en République du Congo: implications hydrogéologique et minière," *Afrique Science*, vol. 16, no. 4, pp. 68-84, 2020.

[43] B. H. Akokponhoué *et al.*, "Contribution of Remote Sensing to the Structural Mapping of Aquifers with Large Water Flows in the Crystalline Hard Rock in the Department of Dongo (North-West of Benin," *International Journal of Emerging Technology and Advanced Engineering*, vol. 12, 2017.

[44] K. G.-C. Douffi, "Distribution spatiale et dynamique de la population de palmiers rôniers, Borassus aethiopum Mart., par

approche de la télédétection et du Système d'Information Géographique (SIG) de la réserve de Lamto (Centre de la Côte d'Ivoire)," PhD Thesis, Université Nangui Abrogoua, Abidjan (Côte d'Ivoire), 2020.

[45] O. Hoarau, "Télédétection et modélisation de populations de moustiques vecteurs: Extraction d'indicateurs paysagers à partir d'images d'Observation de la Terre pour l'estimation de la distribution des gîtes larvaires en milieu urbain," PhD Thesis, Université de la Réunion, 2021.

[46] K. E. G. Kouakou, T. Lasm, B. C. Sombo, M. Y. Ta, D. Baka, and K. E. Kouadio, "Contribution de la géophysique à l'étude structurale et à l'identification des aquifères de fissures dans le Département de Dabakala (Centre-Nord Côte d'Ivoire," vol. 8. p. 18, 2014.

[47] F. Mangolini, J. B. McClimon, F. Rose, and R. W. Carpick, "Accounting for nanometer-thick adventitious carbon contamination in X-ray absorption spectra of carbon-based materials," *Analytical chemistry*, vol. 86, no. 24, Art. no. 24, 2014.

[48] M. Youan Ta, *Contribution de la télédétection et des systèmes d'informations géographiques à la prospection hydrogéologique du socle précambrien d'Afrique de l'Ouest: Cas de la région de Bondoukou Nord Est de la Côte d'Ivoire, cas de la région de Bondoukou (nord-est de la Côte d'Ivoire*. Thèse de Doctorat. Université de Cocody, 2008.

[49] K. Yao, "Hydrodynamisme dans les aquifères de socle cristallin et cristallophyllien du Sud-Ouest de la Côte d'Ivoire : cas du département de Soubré: apports de la télédétection, de la géomorphologie et de l'hydrogéochimie." 2009.

[50] N. Rebouh and A. Khiari, "La Cinematique et l'organisation des structures géologiques dans le Constantinois," 2022.

[51] Y. A. Laaziz, "Contribution des SIG et de la modélisation volumique à la caractérisation géomorphologique et géologique de la région des Doukkala «Meseta côtière, Maroc»-Implication sur les effondrements karstiques," PhD Thesis, université chouaib doukkali, 2021.

[52] C. Bouterid and F. Hafid, "Apports des données lithostratigraphique à la modélisation géologique 3D dans la vallée d'Oued Righ," 2021.

[53] M. Aoudia, A. Issaadi, M. Bersi, D. Maizi, and H. Saibi, "Aquifer characterization using vertical electrical soundings and remote sensing: a case study of the chott Ech Chergui basin, northwest Algeria," *Journal of African Earth Sciences*, vol. 170, p. 103920, 2020.

[54] A. Koudou, B. Adiaffi, and C. C. Kra, "Cartographie des zones de recharge des aquifères de fractures du département de Tanda par analyse multicritère (Nord-Est de la Côte d'Ivoire)," *Bulletin de l'Institut Scientifique, Rabat, Section Sciences de la Terre*, vol. 43, pp. 27-42, 2021.

[55] S. Nakolendousse, S. Yaméogo, A. N. Savadogo, and Y. Koussoube, "Contribution des mesures géophysiques électriques et électromagnétiques dans l'étude du site du barrage de Samendéni: mise en évidence de failles et d'intrusion de dolérites," *Sécheresse*, vol. 20, pp. 232-236, 2009.

[56] B. Adiaffi, "Apport de la géochimie isotopique, de l'hydrochimie et de la télédétection a la connaissance des aquifères de la zone de contact 'socle-bassin sédimentaire' du sud-est de la CÔTE D'IVOIRE," Thése de doctorat, Université Paris Sud - Paris XI, France, 232p. Accessed: Jun. 22, 2021.

[57] M. Y. Laghouag, "Apport de la télédétection (images Landsat 7 ETM+) pour la cartographie géologique de la région d'Aflou". *Atlas saharien*, 2011.

[58] M. Y. Ta, T. Lasm, G. M. Adja, K. J. Kouamé, and J. Biémi, "Cartographie des eaux souterraines en milieu fissuré par analyse multicritère," *Cas de Bondoukou (Côte-d'Ivoire). Revue internationale de géomatique*, vol. 21, pp. 43-71, 2011.

[59] A. P. Sombo, K. É.-G. Kouakou, S. G. Eblin, and B. C. Sombo, "Caractérisation hydrogéologique, par télédétection et géophysique d'accidents régionaux en zone de socle: cas de Sikensi-Tiassalé, Côte d'Ivoire," *Afrique SCIENCE*, vol. 15, pp. 313-327, 2019.

[60] J. Biémi, "Contribution à l'étude géologique, hydrogéologique et par télédétection des bassins versants sub-sahéliens du socle précambrien d'Afrique de l'Ouest: hydrostructurale, hydrodynamique, hydrochimie et isotopie des aquifères discontinus de sillons et aires granitiques de la Haute Marahoué." 1992.

[61] J. P. Jourda, "Méthodologie d'application des techniques de télédétection et des systèmes d'information géographique à l'étude des aquifères fissurés d'Afrique de l'ouest. Concept de l'Hydrotechnique spatiale : cas des zones tests de la Côte d'Ivoire." 2005.

[62] M. Youan Ta *et al.*, "Cartographie des eaux souterraines en milieu fissuré par analyse multicritère. Cas de Bondoukou (Côte-d´Ivoire)," *Revue internationale de géomatique*, vol. 21, no. 1, pp. 43-71, Mar. 2011.

[63] M. Engalenc, "Groundwater in the crystalline basement." CIEH, 1978.

[64] M. Engalenc, "in Role de la fracturation dans la recherche des eaux souterraines dans les granites de l'afrique occidentale", 1975.

[65] A. E. L. Eba *et al.*, "Évaluation De La Vulnerabilite A La Pollution D'une Eau De Surface Destinee A L'adduction D'eau Potable D'une Metropole. Cas De La Lagune Aghein A Abidjan,(Sud De La Cote D'ivoire)," *Eur. Sci. J*, vol. 12, no. 36, pp. 306-326, 2016.

[66] B. Dieng, et al., "Optimisation de l'implantation géophysique des forages en zone de socle au Nord du Burkina Faso." 2004.

[67] K. E. G. Kouakou, L. Dosso, L. N. Kouame, and A. P. Sombo, "in contribution des méthodes de resistivité électrique a la recherche d'eau en milieu cristallin: cas de yakassé-attobrou et d'abié, région de la mé, côte d'ivoire". *18*, 2015.

[68] Y. Koussoube and A. N. Savadogo, "Efficience de trois methodes d'investigation laterale dans la mise en evidence de contacts entre les formations geologiques du proterozoïque inferieur du BURKINA FASO," insu-00947806, Communication, p. 12, 2006.

[69] A. M. Kouassi, K. E. Ahoussi, K. A. Yao, W. Ourega, K. S. B. Yao, and J. Biemi, "Analyse de la productivité des aquifères fissurés de la région du N'zi-Comoé (Centre-Est de la Côte d'Ivoire," *LARHYSS Journal*, p. 1112-3680-2602-7828, 2012.

[70] A. M. Kouassi, K. E. Ahoussi, K. A. Yao, W. Ourega, K. S. B. Yao, and J. Biemi, "Analyse de la productivité des aquifères fissurés de la région du N'zi-Comoé (Centre-Est de la Côte d'Ivoire," *LARHYSS Journal*, p. 1112-3680-2602-7828, 2012.

[71] J. Bordes, "Protection of abstraction points for water intended for human consumption," *Bulletin de liaison du CIEH*, pp. 2-6, 1987.

[72] E. G. K. Kouakou, A. P. Sombo, G. R. Bie, A. K. A. Ehui, and L. N. Kouame, *Comparative study of the results of electrical sounding and drilling logs in basement region. LARHYSS Journal P-ISSN 1112-3680/E-ISSN*, pp. 2602-7828 101-119, 2016.